Textural content in 3T MR: an image-based marker for Alzheimer's disease

S. V. Bharath Kumar[a], Rakesh Mullick[a] and Uday Patil[b]

[a]GE Global Research, John F. Welch Technology Center, Bangalore, India.
[b]Dept. of Radiology, Manipal Hospital, Bangalore, India.

ABSTRACT

In this paper, we propose a study, which investigates the first-order and second-order distributions of T_2 images from a magnetic resonance (MR) scan for an age-matched data set of 24 Alzheimer's disease and 17 normal patients. The study is motivated by the desire to analyze the brain iron uptake in the hippocampus of Alzheimer's patients, which is captured by low T_2 values. Since, excess iron deposition occurs locally in certain regions of the brain, we are motivated to investigate the spatial distribution of T_2, which is captured by higher-order statistics. Based on the first-order and second-order distributions (involving gray level co-occurrence matrix) of T_2, we show that the second-order statistics provide features with sensitivity $> 90\%$ (at 80% specificity), which in turn capture the textural content in T_2 data. Hence, we argue that different texture characteristics of T_2 in the hippocampus for Alzheimer's and normal patients could be used as an early indicator of Alzheimer's disease.

Keywords: Alzheimer's disease, hippocampus, MRI, brain iron, T_2 relaxation, texture, second-order statistics, co-occurrence matrix, image-based marker.

1. INTRODUCTION

Dementia is related to aging, and with the increasing numbers of elderly people in the population, the number of patients with dementia is growing rapidly. The major cause of dementia is Alzheimer's disease (AD). A definite diagnosis of AD relies on histological confirmation at post-mortem or cerebral biopsy, and, therefore, in the majority of cases a definitive diagnosis is not available in life. The diagnosis of AD remains a clinical one with an accuracy of approximately $80\% - 90\%$.[1] With the development of new drug therapies for AD, there has, therefore, been a need to improve the accuracy of diagnosis, particularly in the early stages of the disease when diagnosis is most difficult. Currently there exists no simple test or markers that could detect AD at an early stage. In addition to improving the accuracy of diagnosis of AD, a marker would be valuable in monitoring the progression of the disease, thus aiding in the evaluation of efficacy of therapies.

Excessive iron deposition and increased atrophy in certain regions of the brain such as the hippocampus are known to be the hallmark of AD.[2] Such anomalies in the brains of AD patients leave specific signatures in T_2 images from a magnetic resonance (MR) scan: local excess iron deposition reduces T_2 while local structural anomalies like increased water increase T_2. Thus, compared to normals, T_2 distributions for ADs show thicker lower tails (due to iron) and thicker upper tails (due to increased water content).[3] These differences can be used as a tool to diagnose and monitor AD. Adak *et al.*[3] extracts features related to the lower and upper tails of T_2 distribution for AD detection. Apart from the excessive iron deposition hypothesis, many researchers have studied the volumetrics of different regions of brain as makers for AD detection. MRI studies of regional atrophy in AD suggest that the hippocampus is significantly decreased in volume, whereas other brain regions are less reliable markers of AD.

In this paper, we investigate second-order distributions of T_2 unlike in Adak *et al.*[3] where the first-order distribution of T_2 is studied. The proposed approach is motivated by the desire to capture spatial content of T_2, which is not provided by the first-order statistics as it captures only the gross distribution of data. Since, excess iron deposition occurs locally in certain regions of the brain, it is more appropriate to study the spatial

Send correspondence to S. V. Bharath Kumar, E-mail: bharath.sv@geind.ge.com, Telephone: +91 (80) 2503 3187, Address: Imaging Technologies Lab, General Electric - Global Research, John F. Welch Technology Center, Bangalore-560066, India.

distribution of T_2, which is provided by higher-order statistics. The second-order statistics introduce the context by considering both the present and the past voxel and hence is dependent on the order in which the data is scanned. Since, second-order statistics also capture the textural content present in the given data, investigating the textural information in T_2 might throw some light on the search for a marker for early detection of AD patients. We compute the volumetric texture features using gray level co-occurrence matrix and show that these features outperform the first-order features by providing sensitivity $> 90\%$ at 80% specificity. This study, thus confirms the appropriateness in using second-order statistics for analyzing the excess iron deposition in the hippocampus and provides features which could be used for early detection of AD.

The paper is organized as follows. In Section 2, we provide an overview about statistical approach for texture analysis by introducing first-order and second-order distributions along with gray level co-occurrence matrices. Section 3 presents the details about data set, experimental set up and the method used to determine the texture features. We present the results of our proposed method in Section 4, wherein we compare the performance of second-order texture features with first-order features. We conclude by arguing that the second-order features derived from T_2 data are more appropriate than the first-order features to study excess iron deposition in certain regions of brain and can be used as markers for early detection of Alzheimer's disease.

2. STATISTICAL FEATURES FOR TEXTURE ANALYSIS

Although there is no strict definition of the image texture, it is easily perceived by humans and is believed to be a rich source of visual information about the nature and three-dimensional shape of physical objects. Generally speaking, textures are complex visual patterns composed of entities, or sub-patterns, that have characteristic brightness, color, slope, size, etc. Thus texture can be regarded as a similarity grouping in an image. The local sub-pattern properties give rise to the perceived lightness, uniformity, density, roughness, regularity, linearity, frequency, phase, directionality, coarseness, randomness, fineness, smoothness, granulation, etc., of the texture as a whole.

Different approaches to texture analysis have been investigated in literature, like structural-based approach,[4] statistical-based approach,[5] model-based approach[6,7] and transform-based approach.[8,9] In this paper, we investigate statistical-based approach of texture analysis using first-order and second-order statistics of T_2 images in AD and normal (NL) patients, so as to identify "good" metrics that would aid as markers in detecting early AD cases. In the following sections, we use the terms "image" and "data" to mean T_2 data or image.

2.1. First-order statistics

Let us assume an image of dimensions $N \times M$, to be a function $f(x, y)$ of two space variables x and y, where $x = 0, 1, \cdots, N-1$ and $y = 0, 1, \cdots, M-1$. The function $f(x, y)$ can take discrete values $i = 0, 1, \cdots, G-1$, where G is the total number of intensity levels in the image. The intensity-level histogram is a function showing (for each intensity level) the number of pixels in the whole image, which have this intensity, which is given as

$$h(i) = \sum_{x=0}^{N-1} \sum_{y=0}^{M-1} \delta(f(x, y), i) \tag{1}$$

where $\delta(j, i)$ is the Kronecker delta function:

$$\delta(j, i) = \begin{cases} 1, & j = i \\ 0, & j \neq i \end{cases} \tag{2}$$

The histogram of intensity levels is obviously a concise and simple summary of the statistical information contained in the image. Since, the calculation of the gray level histogram involves single pixels, it contains the first-order statistical information about the image (or its fragment). The probability mass function of occurrence of the intensity levels is obtained by dividing the values $h(i)$ by the total number of pixels in the image.

$$p(i) = \frac{h(i)}{MN}, \quad i = 0, 1, \cdots, G-1 \tag{3}$$

The shape of the histogram provides many clues as to the character of the image. Different useful parameters (image features) can be calculated from the histogram to quantitatively describe the first-order statistical properties of the image, which are mentioned below.

Mean:

$$\mu = \sum_{i=0}^{G-1} ip(i) \tag{4}$$

Variance:

$$\sigma^2 = \sum_{i=0}^{G-1} (i-\mu)^2 p(i) \tag{5}$$

Skewness:

$$\mu_3 = \sigma^{-3} \sum_{i=0}^{G-1} (i-\mu)^3 p(i) \tag{6}$$

Kurtosis:

$$\mu_4 = \sigma^{-4} \sum_{i=0}^{G-1} (i-\mu)^4 p(i) - 3 \tag{7}$$

Energy:

$$E = \sum_{i=0}^{G-1} p^2(i) \tag{8}$$

Entropy:

$$H = -\sum_{i=0}^{G-1} p(i) \log_2 p(i) \tag{9}$$

The mean describes the average level of intensity of the image or texture being examined, whereas the variance describes the variation of intensity around the mean. The skewness is zero if the histogram is symmetrical about the mean, and is otherwise either positive or negative depending on whether it has been skewed above or below the mean. Thus μ_3 is an indication of symmetry. The kurtosis is a measure of flatness of the histogram. The entropy is a measure of histogram uniformity.

2.2. Second-order statistics

The second-order statistics involve context by considering the past pixel, unlike the case in first-order statistics. Hence, the order in which the data or image is scanned becomes important. The second-order histogram is defined as the gray level co-occurrence matrix (GLCM) $h_{d,\theta}(i,j)$. The joint probability mass function, $p_{d,\theta}(i,j)$ of two pixels that are distance d apart along a given direction θ having particular (co-occurring) values i and j is computed by dividing $h_{d,\theta}(i,j)$ by the total number of neighboring pixels in the image. Two forms of co-occurrence matrix exist − one symmetric where pairs separated by d and $-d$ for a given direction θ are counted, and other not symmetric where only pairs separated by distance d are counted. Formally, given the image $f(x,y)$ with a set of G discrete intensity levels, the matrix $h_{d,\theta}(i,j)$ is defined such that its $(i,j)^{th}$ entry is equal to the number of times that $f(x_1,y_1) = i$ and $f(x_2,y_2) = j$, where $(x_2,y_2) = (x_1,y_1) + (d\cos\theta, d\sin\theta)$. This yields a $G \times G$ matrix for each distance d and orientation θ. Different features that describe the second-order properties of the image can be computed from the joint probability mass function, $p_{d,\theta}(i,j)$, which are mentioned below.

Angular Second Moment:

$$s_1 = \sum_{i,j=0}^{G-1} p_{d,\theta}^2(i,j) \tag{10}$$

Correlation:

$$s_2 = \frac{\sum_{i,j=0}^{G-1} ij p_{d,\theta}(i,j) - \mu_x \mu_y}{\sigma_x \sigma_y} \tag{11}$$

Contrast:

$$s_3 = \sum_{i,j=0}^{G-1} (i-j)^2 p_{d,\theta}(i,j) \tag{12}$$

Absolute Value:

$$s_4 = \sum_{i,j=0}^{G-1} |i-j| p_{d,\theta}(i,j) \tag{13}$$

Inverse Difference:

$$s_5 = \sum_{i,j=0}^{G-1} \frac{p_{d,\theta}(i,j)}{1+(i-j)^2} \tag{14}$$

Homogeneity:

$$s_6 = \sum_{i,j=0}^{G-1} \frac{p_{d,\theta}(i,j)}{1+|i-j|} \tag{15}$$

Entropy:

$$s_7 = -\sum_{i,j=0}^{G-1} p_{d,\theta}(i,j) \log_2 p_{d,\theta}(i,j) \tag{16}$$

Maximum Probability:

$$s_8 = \max_{i,j} p_{d,\theta}(i,j) \tag{17}$$

Recursivity:

$$s_9 = \sum_{i=0}^{G-1} \sum_{j=i+1}^{G-1} 4p_{d,\theta}^2(i,j) + \sum_{i=0,\, i=j}^{G-1} p_{d,\theta}^2(i,j) \tag{18}$$

Inverse Recursivity:

$$s_{10} = -\sum_{i=0}^{G-1} \sum_{j=i+1}^{G-1} 2p_{d,\theta}(i,j) \log_2 \left(2p_{d,\theta}(i,j)\right) - \sum_{i=0,\, i=j}^{G-1} p_{d,\theta}(i,j) \log_2 p_{d,\theta}(i,j) \tag{19}$$

μ_x, μ_y, σ_x and σ_y are defined as follows.

$$\mu_x = \sum_{i=0}^{G-1} i p_{d,\theta}^x(i) \tag{20}$$

$$\mu_y = \sum_{j=0}^{G-1} j p_{d,\theta}^y(j) \tag{21}$$

$$\sigma_x^2 = \sum_{i=0}^{G-1} (i-\mu_x)^2 p_{d,\theta}^x(i) \tag{22}$$

$$\sigma_y^2 = \sum_{j=0}^{G-1} (j-\mu_y)^2 p_{d,\theta}^y(j) \tag{23}$$

	Number of cases	Age (yr)	CDR	MMSE
Alzheimer's	24	72.67 ± 4.92	0.63 ± 0.18	24.04 ± 4.24
Normals	17	72.18 ± 6.06	0 ± 0	29.81 ± 0.40

Table 1. Population statistics of an age-matched data set of Alzheimer's and normal patients. CDR (Clinical Dementia Rate) and MMSE (Mini-Mental State Examination) characterize the rate of cognitive decline.

μ_x, σ_x and μ_y, σ_y are the means and standard deviations computed from the marginal densities $p^x_{d,\theta}(i)$ and $p^y_{d,\theta}(j)$ respectively. The marginal densities $p^x_{d,\theta}(i)$ and $p^y_{d,\theta}(j)$ are given as

$$p^x_{d,\theta}(i) = \sum_{j=0}^{G-1} p_{d,\theta}(i,j) \tag{24}$$

$$p^y_{d,\theta}(j) = \sum_{i=0}^{G-1} p_{d,\theta}(i,j) \tag{25}$$

Angular second moment or energy measures the textural uniformity of the image. Absolute value and contrast measure the amount of local variation in the image. Inverse difference and homogeneity measure the smoothness of the data. Entropy measures the disorder of an image and maximum probability results in the pixel pair that is most predominant in the data. Recursivity and inverse recursivity are similar to energy and entropy respectively but account for the symmetric form of GLCM.

The texture features in (10)-(19) can also be extracted from higher order statistical distributions or co-occurrence matrices.[10] The higher-order statistics capture the context information in the image by considering multiple neighboring pixels as against to two as in second-order statistics. Hence, for n^{th} order statistics, the co-occurrence matrix would be of size $G \times G \times \overset{n}{\ldots} \times G$, where G is the number of gray levels in the image. Though higher-order statistics might capture more contextual information in the data than the second-order statistics, they are computationally very intensive and so, in our present study, we restricted ourselves to second-order statistics of T_2 data.

While traditional texture metrics have concentrated on 2-D texture, 3-D imaging modalities are becoming more and more prevalent, providing the possibility of examining texture as a volumetric phenomenon. Just as computer graphics have used 3-D textures as a more realistic alternative to 2-D texture mapping, it is logical to expect that texture derived from volumetric data will have better discriminating power than 2-D texture derived from slice data. Kurani *et al.*[11] extended the co-occurrence matrices for volumetric data, which showed improvements over 2-D texture while trying to characterize the texture of different organs of human body from computed tomography (CT) data. This method involves computing the joint probability mass function, $p_{r,\theta,\phi}(i,j)$ of two voxels that are distance r apart (in 3-D) along an orientation with azimuth angle θ and elevation angle ϕ, having particular co-occurring values i and j. Since $p_{r,\theta,\phi}(i,j)$ is a scaled version of the co-occurrence matrix $h_{r,\theta,\phi}(i,j)$, it is sufficient to compute $h_{r,\theta,\phi}(i,j)$ to capture 3-D textures. Mathematically, the co-occurrence matrix $h_{r,\theta,\phi}(i,j)$ for a given volumetric data $f(x,y,z)$ with a set of G discrete intensity levels is defined such that its $(i,j)^{th}$ entry is equal to the number of times that $f(x_1,y_1,z_1) = i$ and $f(x_2,y_2,z_2) = j$, where $(x_2,y_2,z_2) = (x_1,y_1,z_1) + (r\cos\theta\sin\phi, r\sin\theta\sin\phi, r\cos\phi)$. Again, similar to 2-D textures, this yields a $G \times G$ matrix for each distance r and orientation (θ,ϕ). Different features that describe the 3-D textural properties of the volumetric data can be computed from the joint probability mass function, $p_{r,\theta,\phi}(i,j)$, by substituting $p_{d,\theta}(i,j)$ with $p_{r,\theta,\phi}(i,j)$ in (10)-(19).

3. METHOD

3.1. Patients & Scans

Seventeen normal subjects and 24 probable Alzheimer's patients (on an age-matched basis) are recruited into the study and 3T MRI head scans are acquired for each of these subjects on a General Electric 3T unit. All subjects have consented in accordance with the IRB approved protocol. Dual spin-echo images (TE 18 and 80 ms, TR 5 s, 20 cm FOV, 2 mm slice thickness) are acquired using 3T MRI. Table 1 shows the distribution of

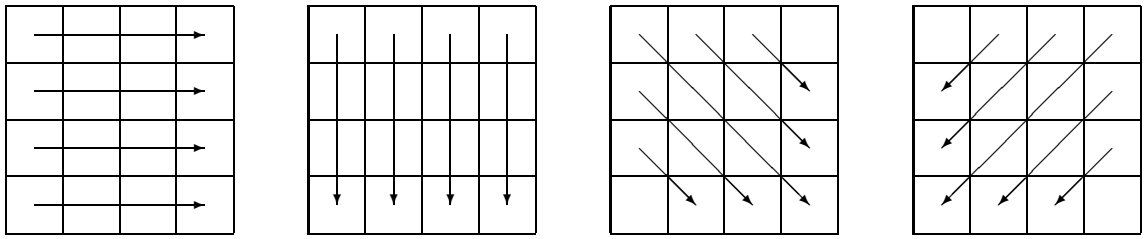

Figure 1. Different scan orders used in the determination of 2-D texture features. (a) $\theta = 0°$, (b) $\theta = 90°$, (c) $\theta = 45°$ and (d) $\theta = 135°$.

Orientation, θ	Displacement vector, $(\Delta x, \Delta y)$
$0°$	$(d, 0)$
$45°$	(d, d)
$90°$	$(0, d)$
$135°$	$(-d, d)$

Table 2. Displacement vectors for co-occurrence matrix in the computation of 2-D textures.

AD and NL patients along with their CDR (clinical dementia rate) and MMSE (mini-mental state examination), which characterize the rate of cognitive decline.

3.2. Texture Analysis of T_2 in the Hippocampus

As mentioned earlier, the underlying idea in investigating the statistics of T_2 images obtained from MRI scans is to study the excessive iron deposition and increased atrophy in certain regions of the brain such as the hippocampus, which are known to be the hallmark of AD. These anomalies in the brains of AD patients leave specific signatures in T_2 images: local excess iron deposition reduces T_2 while structural anomalies like increased water increase T_2.

Since hippocampus is the region of interest in which T_2 statistics need to be investigated, the hippocampus region is manually segmented using AFNI[12] (Analysis of Functional Neuro Images) package. After performing a closing operation to smooth the rough boundary created by manual segmentation, both left and right hippocampi are considered for experimentation along with the corresponding T_2 values in respective regions. The study is carried out by computing the first-order and second-order statistics of T_2 values and then deriving respective metrics for feature selection and classification. The second-order statistics are based on symmetric GLCM, which capture the textural content in T_2 images. The symmetric co-occurrence matrices eliminate the distinction between opposite offset directions, which is appropriate as textures are homogenous by definition. Using these matrices, we investigated both 2-D textures (in each coronal slice of T_2 data) and 3-D textures (over volumetric T_2). For the case of 2-D textures, GLCM with $d = 1, 2, 3, 4, 5$ and $\theta = 0°, 45°, 90°, 135°$ is computed for each coronal slice, resulting in $10 \times 5 \times 4 = 200$ features per slice. Figure 1 shows the scan order involved in the computation of 2-D textures. Table 2 shows the displacement vector $(\Delta x, \Delta y)$ for co-occurrence matrix as a function of d for various θ in the computation of 2-D textures.

In the computation of 3-D texture features for volumetric T_2, GLCM with $r = 1, 2, 3, 4, 5$ and $\theta, \phi = 0°, 45°, 90°, 135°$ is computed for the whole volume unlike 2-D textures, which are computed for each coronal slice. Table 3 shows the displacement vector $(\Delta x, \Delta y, \Delta z)$ for co-occurrence matrix as a function of r for various θ and ϕ in the computation of 3-D textures. Assuming a volumetric data of K slices, 2-D texture computation requires K co-occurrence matrices resulting in $200K$ features. On the other hand, 3-D textures require computation of 1 co-occurrence matrix resulting in $10 \times 5 \times 13 = 650$ features. The 3-D texture method not only captures better textural content but also is computationally cheap compared to 2-D texture method.

While computing features using 3-D texture method, we also investigated two variations in the range of T_2 over which the co-occurrences matrices are computed.

Orientation, (θ, ϕ)	Displacement vector, $(\Delta x, \Delta y, \Delta z)$
$(0°, 45°)$	$(r, 0, r)$
$(0°, 90°)$	$(r, 0, 0)$
$(0°, 135°)$	$(r, 0, -r)$
$(45°, 45°)$	(r, r, r)
$(45°, 90°)$	$(r, r, 0)$
$(45°, 135°)$	$(r, r, -r)$
$(90°, 45°)$	$(0, r, r)$
$(90°, 90°)$	$(0, r, 0)$
$(90°, 135°)$	$(0, r, -r)$
$(135°, 45°)$	$(-r, r, r)$
$(135°, 90°)$	$(-r, r, 0)$
$(135°, 135°)$	$(-r, r, -r)$
$(-, 0°)$	$(0, 0, r)$

Table 3. Displacement vectors for co-occurrence matrix in the computation of 3-D textures.

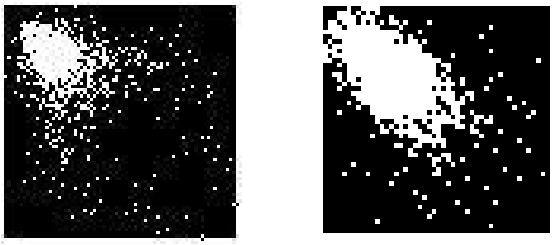

Figure 2. Gray level co-occurrence matrix (shown in gray scale) of volumetric T_2 in the right hippocampus for (a) Alzheimer's patient and (b) Normal patient. It is clear from the figure that 3-D textures would provide good discrimination between Alzheimer's and normal patients.

1. $0 \leq T_2 \leq \max(T_2)$
2. $0 \leq T_2 \leq 80\,\text{ms}$

Since, low T_2 values reflect the brain iron concentration which is understood to be an indicator of AD, we are motivated to investigate the second-order distribution of T_2 in its lower range, i.e. $0 \leq T_2 \leq 80\,\text{ms}$ apart from studying its second-order distribution over the entire range. Figure 2 shows the co-occurrence matrices of volumetric T_2 in the right hippocampus for both AD and NL patients. It is clear from Figure 2 that the co-occurrence matrices are quite different for AD and NL and so one would expect the features derived from these matrices to provide good separability between AD and NL. In the next section, we discuss the analysis of features generated from first-order, 2-D and 3-D textures and show that 3-D textures provide better separability between AD and NL and hence could be used as a marker in the early detection of AD.

3.3. Feature Selection and Classification

As aforementioned, we computed 200 2-D texture features (averaged over coronal slices) and 650 3-D texture features for each of right and left hippocampi based on the second-order statistics of T_2 data. Since the feature space is prohibitively large, a parsimonious representation of the feature space is needed for better classification performance. To achieve the same, we carried out ROC (receiver operating characteristic) analysis for each of the features and the ones that provide high sensitivities at 80% specificity are selected as probable markers for early AD detection.

The ROC analysis is commonly used to measure the performance of a two-class classification problem. In our case, each feature is analyzed independently using a threshold classifier, in which a hypothetical Alzheimer's

case is classified as an "Alzheimer's" (or "normal") if the value of the feature is below (or above) a threshold value. The ROC curve represents a *sensitivity* (S) versus *1-specificity* ($1 - S'$), defined as

$$S = \frac{TP}{TP + FN} \tag{26}$$

$$S' = \frac{TN}{TN + FP} \tag{27}$$

where TP is the number of true positives (correctly detected AD cases), TN is the number of true negatives (correctly detected NL cases), FP is the number of false positives (NLs classified as AD cases) and FN is the number of false negatives (AD cases classified as NLs). Ideally one would require $S = 1$ and $S' = 1$, which means that all AD cases are detected without any false positives. The ROC curve makes it possible to evaluate the performance of the detection process at different points of operation (as defined for example by means of classification thresholds). The area under the ROC curve (A_{roc}) is normally used as a measure of this performance as it indicates how the detection of AD cases can be carried out: a value of $A_{roc} = 1$ indicates an ideal detection, while a value of $A_{roc} = 0.5$ corresponds to random classification.

4. RESULTS

The ROC analysis is conducted on the first-order and second-order statistical features with an aim to reduce the feature space and also to select the features that provide high values of sensitivity (at 80% specificity) and A_{roc}. Higher the value of sensitivity and A_{roc}, better is the classification rate and higher is the chance of using such a feature as a marker for early AD detection. Figure 3 and Figure 4 show the sensitivity and A_{roc} performance of first-order and second-order statistical features computed from T_2 data in the right hippocampus for an age-matched cohort of AD and NL patients. The following second-order features,

1. Angular second moment (s_1)
2. Contrast (s_3)
3. Absolute value (s_4)
4. Inverse difference (s_5)
5. Homogeneity (s_6)
6. Maximum probability (s_8)

computed on volumetric T_2 for two different ranges perform better than 2-D texture features and first-order features. Also, these features show significantly higher performance along $(\theta, \phi) = (0°, 90°), (45°, 135°), (90°, 135°), (135°, 135°)$ and $r = 2, 3, 4$ compared to other orientations. Though the second-order features are dependent on (d, θ) or (r, θ, ϕ), we have not shown their dependence in Figure 3 and Figure 4. The sensitivity and A_{roc} values shown in Figure 3 and Figure 4 respectively are the average of values along the aforementioned (r, θ, ϕ). Interestingly, similar performance is achieved by the second-order features in the left hippocampus also, which is shown in Figure 5 and Figure 6. It is to be noted from Figure 3 to Figure 6 that the performance of the 3-D texture features over $0 \leq T_2 \leq 80$ ms is slightly better than the performance with entire T_2, which in a way supports the hypothesis of excessive iron deposition in the hippocampus. The experiment with 2-D textures is conducted to prove that second-order statistics are more appropriate to capture the spatial content in T_2, which is absent in the first-order statistics. Since, 2-D textures do not capture the spatial information along coronal direction, we use 3-D textures to exploit the textural information present in T_2 along that direction. This study, thus confirms the appropriateness in using second-order statistics for analyzing the excess iron deposition in the hippocampus and provides features which could be used for early detection of AD. The abscissa in Figure 3 to Figure 6 shows two features (first-order/second-order), which need to be considered according to the feature under investigation. The sensitivity and A_{roc} values of s_4 for 2-D textures are not shown in Figure 3 to Figure 6 as its average value is less than 20%. Hence, s_4 is not chosen as a marker in the AD detection when 2-D texture method is used.

Since Freeborough *et al.*[1] have shown good classification results between AD and NL using T_1-weighted data from 1.5T MRI, we conducted similar study on T_1 data from 3T MRI using second-order statistics. Our study on T_1 provided a maximum sensitivity of 60% at a specificity of 80% and did not turn out to be a good metric for early AD classification.

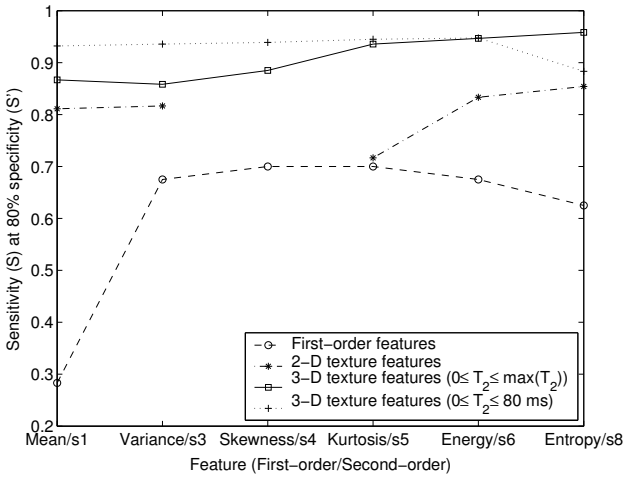

Figure 3. Sensitivity (S) at 80% specificity (S') for first-order and second-order T_2 features computed in the right hippocampus. The second-order features involve computation of 2-D and 3-D textures. The 3-D textures are investigated over two different ranges of T_2. It is clear from the figure that 3-D textures outperform both 2-D textures and first-order features, thus supporting the brain iron hypothesis. Refer (4)-(19).

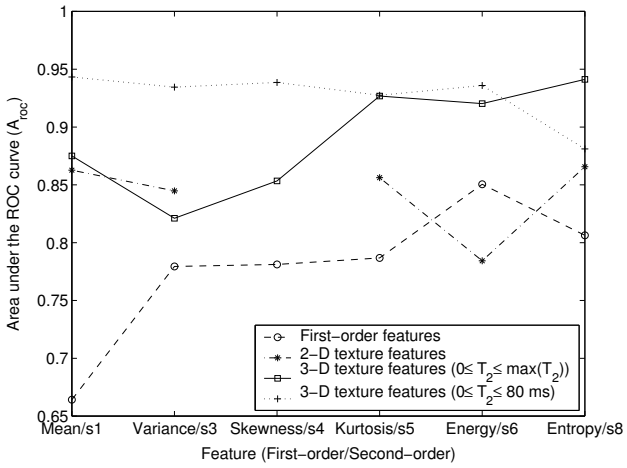

Figure 4. Area under the ROC curve (A_{roc}) for first-order and second-order T_2 features computed in the right hippocampus. The second-order features involve computation of 2-D and 3-D textures. The 3-D textures are investigated over two different ranges of T_2. It is clear from the figure that 3-D textures outperform both 2-D textures and first-order features, thus supporting the brain iron hypothesis. Refer (4)-(19).

5. CONCLUSION

We presented a novel study, which investigates the textural content of T_2 values for Alzheimer's and normal patients and provides features which could turn out to be early indicators of AD. The study is motivated by the desire to analyze the local brain iron uptake in Alzheimer's patients, which is captured by low T_2 values. We investigated the first-order and second-order statistics of T_2 data and showed that the second-order statistics provide features with high sensitivities ($> 90\%$ at 80% specificity) and in turn capture the textural content of T_2 data in the hippocampus. This study also confirms the appropriateness in using second-order statistics over first-order statistics to analyze the excess iron deposition in the hippocampus. Though, visually, we do not perceive any textural pattern in the T_2 data, the study confirms the existence of some texture pattern in T_2 data. Hence, a better understanding is needed to correlate the study to either brain iron or atrophy or other biological markers. Similar study on T_1 data did not provide good markers for AD detection.

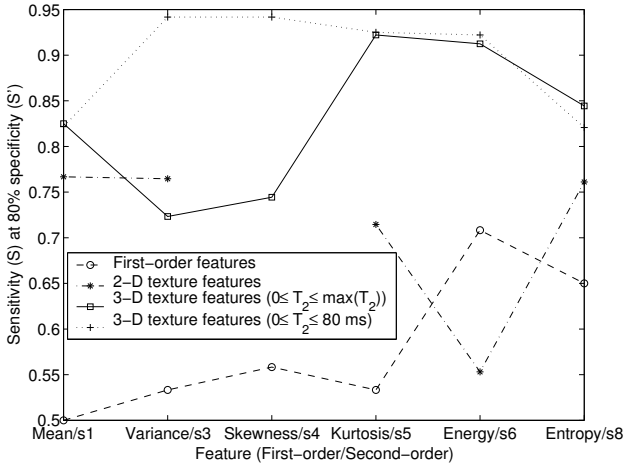

Figure 5. Sensitivity (S) at 80% specificity (S') for first-order and second-order T_2 features computed in the left hippocampus. The second-order features involve computation of 2-D and 3-D textures. The 3-D textures are investigated over two different ranges of T_2. It is clear from the figure that 3-D textures outperform both 2-D textures and first-order features, thus supporting the brain iron hypothesis. Refer (4)-(19).

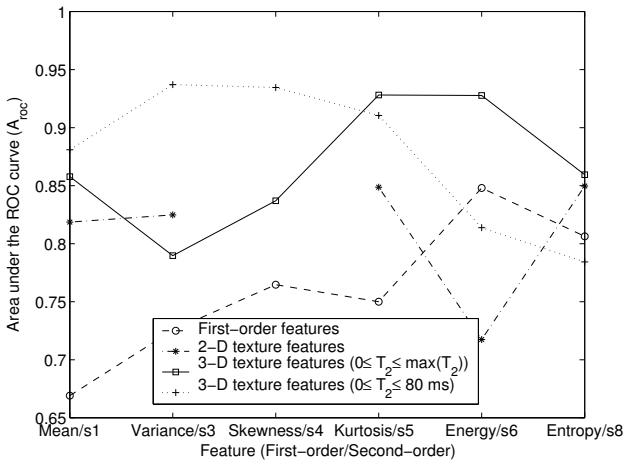

Figure 6. Area under the ROC curve (A_{roc}) for first-order and second-order T_2 features computed in the left hippocampus. The second-order features involve computation of 2-D and 3-D textures. The 3-D textures are investigated over two different ranges of T_2. It is clear from the figure that 3-D textures outperform both 2-D textures and first-order features, thus supporting the brain iron hypothesis. Refer (4)-(19).

REFERENCES

1. P. A. Freeborough and N. C. Fox, "MR image texture analysis applied to the diagnosis and tracking of Alzheimer's disease," *IEEE Transactions on Medical Imaging* **17**, pp. 475–479, June 1998.
2. A. M. Alyassin, J. F. Schenck, Z. Li, D. C. Alsop, and E. A. Zimmerman, "Brain iron analysis of high field MR images for Alzheimer's disease," –.
3. S. Adak, A. Saha, S. Paul, R. Tandon, B. O. Narayanan, W. P. Gorman, J. F. Schenck, Z. Li, T. O'Keefe, and E. A. Zimmerman, "Classification of Alzheimer's disease using T_2 distribution parameters from 3T MRI," –.
4. R. M. Haralick, "Statistical and structural approaches to texture," *Proceedings of the IEEE* **67**(5), pp. 786–804, 1979.

5. R. M. Haralick, K. Shanmugam, and I. Dinstein, "Textural features for image classification," *IEEE Trans. on Systems, Man, and Cybernetics* **SMC-3**, pp. 610–621, November 1973.
6. G. C. Cross and A. K. Jain, "Markov random field texture models," *IEEE Transactions on Pattern Analysis and Machine Intelligence* **PAMI-5**, pp. 25–39, 1983.
7. J. M. Keller, S. Chef, and R. M. Crossover, "Texture description and segmentation through fractal geometry," *Computer Vision, Graphics, and Image Processing* **45**, pp. 150–166, 1989.
8. M. R. Turner, "Texture discrimination by gabor functions," *Biological Cybernetics* **55**, pp. 71–82, 1986.
9. T. Chang and C. C. J. Kuo, "Texture analysis and classification with tree-structured wavelet transform," *IEEE Transactions on Image Processing* **2**, pp. 429–441, October 1993.
10. V. A. Kovalev, F. Kruggel, H. J. Gertz, and D. Y. Cramon, "Three-dimensional texture analysis of MRI brain datasets," *IEEE Trans. on Medical Imaging* **20**, pp. 424–433, May 2001.
11. A. Kurani, D. H. Xu, J. Furst, and D. S. Raicu, "Co-occurrence matrices for volumetric data," in 7^{th} *IASTED International Conference on Computer Graphics and Imaging*, (Hawaii, USA), 2004. submitted.
12. R. W. Cox, "AFNI: Software for analysis and visualization of functional magnetic resonance neuroimages," *Computers and Biomedical Research* **29**, pp. 162–173, 1996.